IEEE INSTRUMENTATION & MEASUREMENT SOCIETY

Received 26 July 2022; accepted 24 August 2022. Date of publication 1 September 2022; date of current version 20 September 2022.
The review of this article was arranged by Associate Editor Paolo Attilio Pegoraro.

Digital Object Identifier 10.1109/OJIM.2022.3203444

Three-Phase Electrical Measurement Representations for Nonintrusive Load Diagnostics

DAISY H. GREEN [1] (Member, IEEE), PETER A. LINDAHL [2] (Senior Member, IEEE), AND STEVEN B. LEEB [3] (Fellow, IEEE)

[1]Department of Architecture, Massachusetts Institute of Technology, Cambridge, MA 02139, USA

[2]Exponent, Inc., Natick, MA 01760, USA

[3]Department of Electrical Engineering and Computer Science, Massachusetts Institute of Technology, Cambridge, MA 02139, USA.

CORRESPONDING AUTHOR: D. H. GREEN (e-mail: dhgreen@mit.edu)

This work was supported in part by the Office of Naval Research NEPTUNE Program and in part by The Grainger Foundation.

ABSTRACT Electromechanical systems experience both gradual and sudden fault conditions. Power monitoring provides a valuable approach for detecting faults, essentially turning a machine into its own sensor for observing developing and abrupt failures. Machines can be monitored individually or nonintrusively (as a collection of loads) and signal processing can tease out relevant indicators of operational status and health. Load identification and diagnostics with aggregate electrical monitoring rely on the correct physical interpretation of measurements. Specifically, ties between the observed measurements and the actual physical task performed by a load ensure the relevance of a measurement, or a feature space derived from the measurement, for reliable identification and diagnostics. This article examines three-phase mathematical relationships for different load configurations, specifically with an eye toward selecting a feature space useful for automated diagnostics. The utility of these three-phase measurement representations is demonstrated with experimental data from several microgrid systems.

INDEX TERMS Fault detection, load identification, nonintrusive load monitoring, power measurement.

I. POWER AS PREDICTOR

EFFORTS to automate the operation of industrial and transportation systems with advanced controls and electromechanical actuators underscore a need for accurate fault detection and diagnostics (FDD) [1]. Feedback control and automation hides the prevalence of "soft faults," or the gradual degradation of system performance. For instance, an electrical load can experience various deviations from expected healthy behavior due to aging, corrosion, and mechanical failure [2], [3]. Soft faults reduce energy efficiency, hide electrical safety hazards, and eventually lead to a "hard fault" that takes operating machinery offline. Electrical monitoring can provide diagnostic indicators for identifying soft faults.

A nonintrusive load monitor (NILM) is a convenient approach for electrical monitoring, as it uses a single set of current and voltage sensors to monitor a collection of loads [4]. With correct interpretation, data from a NILM can identify healthy versus faulty behavior and supplement existing protection schemes. Machine learning systems essentially seek correlations between input data and training classifications or categories [5]. The presentation of input data characteristics, i.e., the "feature space" used to describe a problem or dataset, can greatly affect training effort, operating speed, and identification accuracy [6]. The "Achilles heel" of machine learning systems is the quality and presentation format of input data for training and operations. The training data for a nonintrusive load monitoring classifier is unlikely to contain instances of possible fault conditions. Given a limited training dataset, it is crucial for the feature space to be physically informed. An understanding of the physical mechanisms for possible faults can be used to inform a feature space useful for nonintrusive load FDD.

A polyphase system presents additional challenges for load identification and diagnostics, in part due to potential imbalances in the system. For example, a three-phase system can have an unbalanced generation system (i.e., unbalanced supply voltages) and unbalanced loads (i.e., loads are not evenly distributed among the phases). Unbalanced voltages can have detrimental impacts on connected equipment and result in deviations in expected load behavior [7]. An unbalanced load

system is also a power quality concern; however, load imbalance does not necessarily indicate improper individual load operation. A healthy load is one that is operating according to design specifications. A healthy load does not imply a balanced load system, and a balanced load is not necessarily a healthy load.

This article presents three-phase measurement representations and mathematical relationships for attributing load transient behavior, such as when a load energizes or changes state, to healthy or faulty load operation. The work in this article extends on the previous work that uses aggregate electrical monitoring for FDD [8], [9], [10], [11], [12], [13]. Particularly, the work in [9] and [8] is focused on detecting anomalous load cycling. However, these works do not consider changing power characteristics, such as transient or steady-state behavior. The work in [10] and [11] uses changes in steady-state power as a diagnostic metric by creating warning threshold levels based on historical data. However, to characterize load behavior based on historical data, it could require months or years of data collection. The method demonstrated in [12] can adapt to drifting load power characteristics, even with a limited training dataset. However, the method is limited to gradual load drift and requires outside supervision if an abrupt fault occurs. Furthermore, the diagnostic metrics in [8], [9], [10], [11], and [12] are not specific to three-phase or polyphase systems, and as a result, they do not fully consider imbalances in the system. Reference [13] presents electrical observations and "root-cause" failure analysis for a specific piece of industrial equipment, a three-phase immersion heater. Three-phase immersion heaters are also included as examples in this article, along with several other loads, to illustrate the value of a proper physically informed feature space for FDD.

The work in this article is specifically focused on measurement interpretation for load diagnostics in three-phase systems and the challenges and opportunities that arise. Changes in system balances for currents, voltages, and harmonic content, particularly during load turn on and turn off transients, form a useful feature space for FDD. Changes in balances that occur during transients tend to be associated with the particular load change under observation and can be distinguished from an arbitrary background imbalance in the power system. This article demonstrates techniques with applicability across polyphase power systems for defining a feature space useful for nonintrusive load FDD. Examples are illustrated with measurements made on several marine delta-configured systems.

II. THREE-PHASE METERING

There are various power system configurations, including single phase, split phase (single-phase three wire), and three phase. Three-phase systems can be three-wire, four-wire, or five-wire, depending on the neutral and ground connections. There are also configurations such as a high-leg delta, where the center point of one phase is grounded. A NILM can monitor any of these systems. However, measurements are also limited by physical access and convenience. An example that illustrates this is a three-wire delta system, commonly used industrially and especially on ships. For instance, measurements of phase currents (i.e., the current through the load) of delta-connected loads are unlikely to be made nonintrusively. It is more likely to have nonintrusive access to line currents (i.e., the currents in the line conductors). For FDD, it is useful to have all three line currents, e.g., if there are current imbalances or a bonding fault. There is valuable reexamination to be done for considering the feature space that is best suited for connecting measured power and harmonic consumption to physical performance. The ideas discussed in this article are demonstrated with NILM systems that have been installed on various shipboard microgrids. These microgrids are ungrounded delta-distributed systems with wye-configured source generators.

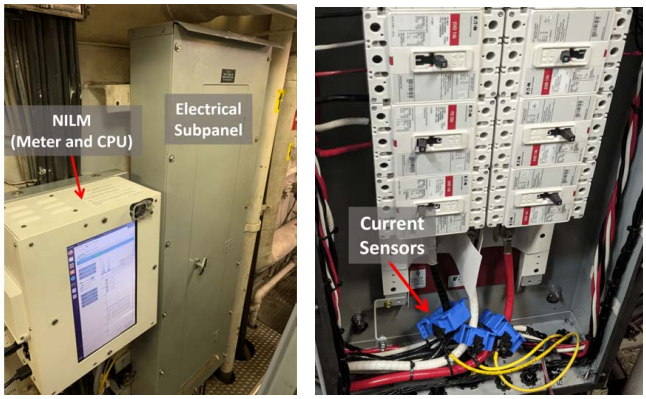

FIGURE 1. NILM installation on USCGC THUNDER BAY: (a) NILM box containing meter and CPU mounted next to the monitored electrical panel and (b) electrical panel interior with installed current sensors.

The shipboard NILM systems measure three line-to-line voltages and three line currents. Fig. 1 shows a NILM installation onboard U.S. Coast Guard Cutter (USCGC) THUNDER BAY. Fig. 1(a) shows a NILM box, which contains the NILM meter and computer processing and storage unit (CPU). This NILM box is mounted directly next to the monitored electrical subpanel. The NILM meter contains the analog circuitry and the LabJack UE9 [14] data acquisition (DAQ) hardware. This DAQ obtains data at a 12-bit input resolution. An analog-to-digital converter (ADC) samples the voltages and currents at 8 kHz. The current sensing hardware is either the LEM LF-305 or LF-505 [as shown in Fig.1(b)], which can measure currents up to 300 and 500 A, respectively. The NILM software is run on a Linux-based personal computer [4] and data is displayed to the user via a touchscreen interface.

A. THREE-PHASE POWER

For nonsinusoidal and unbalanced polyphase systems, there is currently no agreement on a universally applicable power theory [15], [16], [17], [18], [19]. There are various analysis tools and transformations used for calculating power and

detecting imbalances, useful for different applications such as energy billing, power quality evaluation, and design of active filters. Instantaneous pq theory, for example, was formulated for the control of switching compensators, known as "active power filters" [15]. This theory is based on the $\alpha\beta 0$ transform (the Clarke transform) to transform three-phase (abc) voltages and currents into the $\alpha\beta 0$ stationary reference frame [15]. Another common transform is the Park transform, which is used to convert three-phase ac waveforms into a rotating reference frame with direct, quadrature, and zero components ($dq0$), such that they can be analyzed as dc signals. This transform is often used in the modeling and control of three-phase electric machines and three-phase inverters [20]. The method of symmetrical components was formulated for analyzing unbalanced power system operation. Symmetrical components convert a three-phase unbalanced system into two sets of balanced phasors (i.e., positive and negative sequence components) and a set of phasors which are in-phase with each other (i.e., zero-sequence components) [21]. This technique is typically used in the analysis of unbalanced short-circuit faults and unbalanced operation of induction machines [20], [22]. For stability and dynamic analysis of relatively slow transients, time-varying phasor analysis is often used [23].

The work in this article uses the "spectral envelope" representation of current and voltage signals, which are short-term averages of the harmonic content at integer multiples of the ac line frequency [24]. The applicability of spectral envelopes for nonintrusive load monitoring and transient identification has been demonstrated in [24], [25], and [26]. This method assumes that the voltage and current signals are locally periodic over one ac line cycle. This time-varying spectral envelope representation is beneficial in that it compresses the 8-kHz current and voltage data into 60-Hz power and higher order current harmonic streams, while preserving important amplitude, phase, and harmonic information. Furthermore, voltages and currents are converted into a form in which an edge detector or change-of-mean detector can easily be run to detect load transients. When focused on approximately linear loads during steady-state operation, the expected per-phase power for certain load and fault conditions are derived from phasor analysis and compared to the spectral envelope power streams.

B. MEASUREMENT PREPROCESSING

Without access to measurable line-to-neutral voltages, the voltages are assumed harmonic-free (i.e., containing only the fundamental component). The line-to-neutral voltages can be represented as

$$\begin{aligned} v_a(t) &= V_a \cos(\omega t + \theta_a) \\ v_b(t) &= V_b \cos\left(\omega t - \frac{2\pi}{3} + \theta_b\right) \\ v_c(t) &= V_c \cos\left(\omega t + \frac{2\pi}{3} + \theta_c\right) \end{aligned} \tag{1}$$

where V_a, V_b, and V_c are the peak magnitudes, θ_a, θ_b, and θ_c are the phase angles, and ω is the angular frequency. Further assuming a balanced system, $V_a = V_b = V_c = V_{pk}$ and $\theta_a = \theta_b = \theta_c = 0$. For a single frequency component, the voltages can be represented in phasor notation. The line-to-neutral and line-to-line voltages are

$$\begin{aligned} \mathrm{v_a} &= V & \mathrm{v_{ab}} &= \sqrt{3}Ve^{j\frac{\pi}{6}} \\ \mathrm{v_b} &= Ve^{-j\frac{2\pi}{3}} & \mathrm{v_{bc}} &= \sqrt{3}Ve^{-j\frac{\pi}{2}} \\ \mathrm{v_c} &= Ve^{j\frac{2\pi}{3}} & \mathrm{v_{ca}} &= \sqrt{3}Ve^{j\frac{5\pi}{6}} \end{aligned} \tag{2}$$

where V is the rms line-to-neutral voltage (i.e., $V = V_{pk}/\sqrt{2}$). The line currents at line-frequency harmonic k can be represented as

$$\begin{aligned} i_{ak}(t) &= A_{ak} \cos(k\omega t + \delta_{ak}) \\ i_{bk}(t) &= A_{bk} \cos\left(k\left(\omega t - \frac{2\pi}{3}\right) + \delta_{bk}\right) \\ i_{ck}(t) &= A_{ck} \cos\left(k\left(\omega t + \frac{2\pi}{3}\right) + \delta_{ck}\right) \end{aligned} \tag{3}$$

where A_{ak}, A_{bk}, and A_{ck} are the peak magnitudes and δ_{ak}, δ_{bk}, and δ_{ck} are the phase angles.

To detect load transient behavior, the available measurements are first preprocessed into spectral envelopes. This process, as described below, is also presented in [13]. Spectral envelopes of the currents are computed over sliding windows of the input signal phase-aligned with a reference voltage, $v[n] = V_{pk}\sin(2\pi n/N)$. Given a sampling frequency f_s and line frequency f_0, one period is length $N = f_s/f_0$ samples. Under the assumption that the voltages are relatively "stiff" and harmonic-free, a single measured line-to-line voltage can be used as the phase reference.

For a current $i[n]$, in which the current is phase-aligned with the reference voltage, the in-phase and quadrature components of the rms current envelope at line frequency harmonic k are

$$I_k^I = \frac{\sqrt{2}}{N}\sum_{n=0}^{N-1} i[n]\sin\left(k\frac{2\pi n}{N}\right) \tag{4}$$

$$I_k^Q = -\frac{\sqrt{2}}{N}\sum_{n=0}^{N-1} i[n]\cos\left(k\frac{2\pi n}{N}\right). \tag{5}$$

These are equivalent to the imaginary and real components, respectively, of the discrete Fourier transform (DFT) of $i[n]$, scaled by $-\sqrt{2}/N$. A block diagram of the data preprocessing for calculating current spectral envelopes is shown in Fig. 2. Since only one voltage is used as the phase reference, phase rotation corrections need to be applied. A correcting rotation of $k\psi_0$ can be applied to the complex DFT coefficient X_k as $X_k \cdot e^{\psi_0 \cdot jk}$. When the voltages are measured line-to-line, phase rotations of 30°, 150°, and 270° should be applied, corresponding to $i_a[n]$, $i_b[n]$, and $i_c[n]$, respectively. If there is a phase shift of 180° of the voltages with respect to the currents, phase rotations of 210°, 330°, and 90° should be applied instead. The in-phase and quadrature spectral envelopes for each phase $\psi \in \{a, b, c\}$ are represented as $I_{\psi k}^I$ and $I_{\psi k}^Q$, respectively. The fundamental current component is used to calculate the real power (P) and reactive

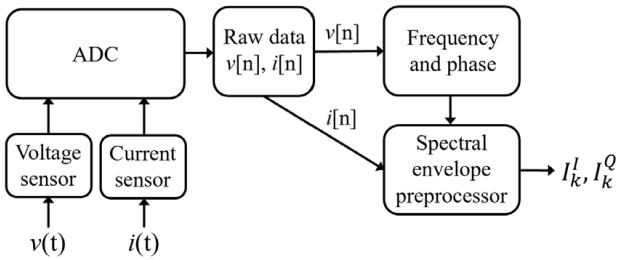

FIGURE 2. Block diagram of the DAQ and preprocessing stages (adapted from [25]).

power (Q) streams for each phase

$$P_\psi = VI^I_{\psi 1}, \quad Q_\psi = VI^Q_{\psi 1} \tag{6}$$

where the rms line-to-neutral voltage is assumed a constant V. For the evaluation of voltage imbalance, spectral envelopes can also be computed for the line-to-line voltages. From the computed "per-phase" power and higher order harmonic current envelopes, a feature space can be extracted.

III. LOAD IMBALANCE FEATURE SPACE

Pattern classifiers need to disaggregate both healthy and faulted loads from the aggregate power stream. The installed NILM systems use an edge detector [27] to find load events, such as load on and off events and transitions between discrete states. At each event, a set of extracted features is used for load identification [28]. The preprocessing in Section II computes the per-phase power and higher order current harmonics. Thus, features extracted from the per-phase power and higher order current harmonics, such as steady-state and inrush characteristics, are an intuitive choice of features for load identification [28]. However, the following questions should be considered when assessing the usefulness of a feature space for load diagnostics if the load experiences gradual degradation or a sudden fault.

- How do the changes manifest in the feature space?
- Are the changes in the feature space physically interpretable?
- Is the load still uniquely identifiable?

These questions are especially important in a three-phase system because of the inherent imbalances of certain load and fault types. Without a physics-informed feature space, it is difficult to correctly attribute imbalances to the correct load. The loads monitored in this work are connected line-to-line. Thus, the power consumption on each delta phase (i.e., *ab*, *bc*, and *ca*) may be more intuitive for interpreting load changes. Computing the power per delta phase requires knowing the phase currents. However, from the line currents of a delta-connected system, and without making any further assumptions, it is not possible to calculate the true delta phase currents. The line currents are governed by the following relationships, where the matrix is not invertible:

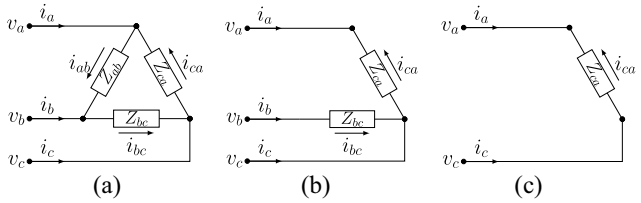

FIGURE 3. Conceptual diagrams for three possible load connection types in a delta-connected system: (a) three delta phases, (b) two delta phases, and (c) single delta phase, with line currents i_a, i_b, and i_c and phase currents i_{ab}, i_{bc}, and i_{ca}.

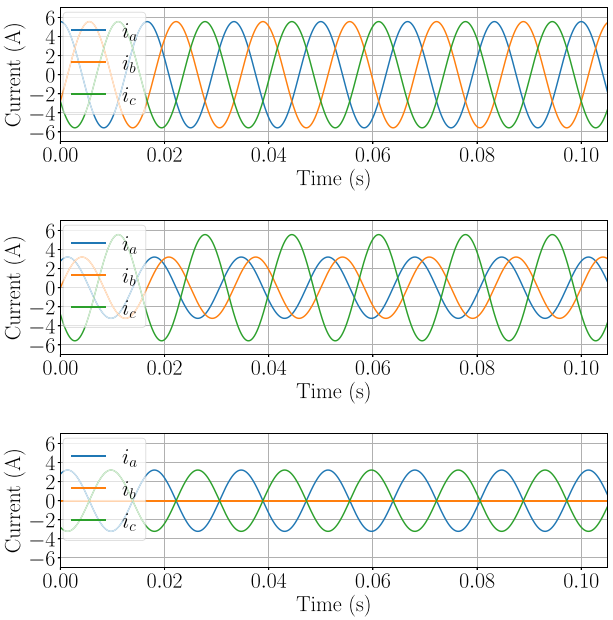

FIGURE 4. Line currents for three different load connections in a delta-connected system: three delta phases (top), two delta phases (middle), and a single delta phase (bottom).

$$\begin{bmatrix} i_a \\ i_b \\ i_c \end{bmatrix} = \begin{bmatrix} 1 & 0 & -1 \\ -1 & 1 & 0 \\ 0 & -1 & 1 \end{bmatrix} \begin{bmatrix} i_{ab} \\ i_{bc} \\ i_{ca} \end{bmatrix}. \tag{7}$$

To resolve the nonuniqueness of possible phase currents, this work proposes a feature set based on an assumption that loads are connected in one of the three ways in the monitored delta-configured system: 1) three delta phases; 2) two delta phases; or 3) a single delta phase. Every step change in power can first be evaluated to determine if the relative balance or imbalance is consistent with that of an expected load connection type. The ship systems monitored in this work did not contain any delta two-phase loads. Thus, a transient that results in imbalances consistent with a delta two-phase load is considered a fault condition of a three-phase load, such that one of the delta phases open-circuited. A load identified as connected on a single delta phase can either be a normally operating single-phase load or a fault condition of a three-phase load. Conceptual diagrams for examples of these three connection types are shown in Fig. 3. Example line currents are shown in Fig. 4 for resistances of 193.6 Ω

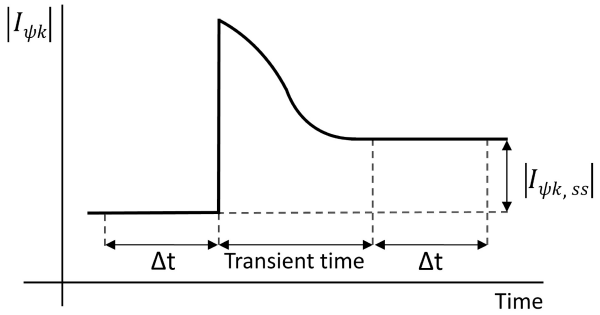

FIGURE 5. Conceptual diagram of steady-state calculation.

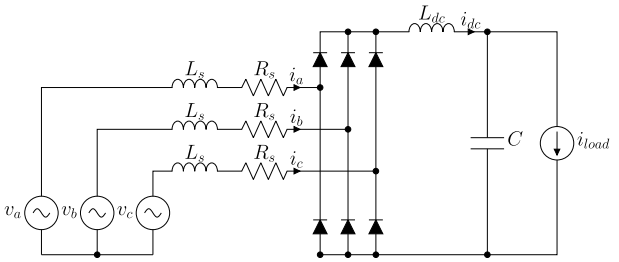

FIGURE 6. Three-phase uncontrolled diode bridge rectifier with inverter-motor combination modeled as current source.

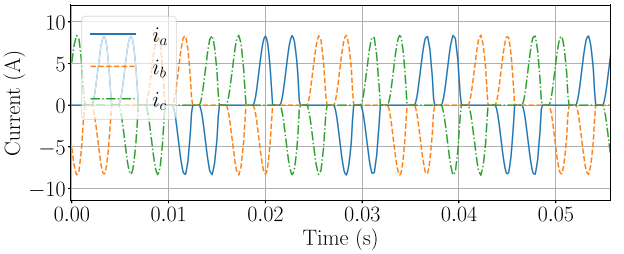

FIGURE 7. Line currents of a simulated 1-kW load controlled by a VFD.

(corresponding to 1 kW per delta phase on a 440/254-V system).

With this assumption, the ratios of fundamental line current spectral envelope magnitudes can be used to determine the load connection type and, subsequently, the estimated phase currents. The magnitudes of the spectral envelopes are computed as

$$|I_{\psi k}| = \sqrt{\left(I^I_{\psi k}\right)^2 + \left(I^Q_{\psi k}\right)^2}. \tag{8}$$

At every detected event, the change in steady-state magnitude, $I_{\psi 1,ss}$, is calculated for each phase as the difference in medians (or alternatively, the means) of Δt windows before and after the event, as illustrated in Fig. 5. The relative magnitudes of the three line currents can now be computed

$$\left[\left|\frac{I_{a1,ss}}{I_{b1,ss}}\right|, \quad \left|\frac{I_{b1,ss}}{I_{c1,ss}}\right|, \quad \left|\frac{I_{c1,ss}}{I_{a1,ss}}\right|\right]. \tag{9}$$

Alternatively, the ratios can be computed using the per-phase apparent power streams (i.e., $S_\psi = \sqrt{P^2_\psi + Q^2_\psi}$) since P_ψ and Q_ψ are scaled versions of $I^I_{\psi 1}$ and $I^Q_{\psi 1}$, respectively, as defined in (6). These ratios present a measure of load balance or imbalance. The next two sections demonstrate how these ratios, in conjunction with power consumption, can help distinguish healthy versus faulty behavior.

IV. BALANCED THREE-PHASE LOADS

A balanced three-phase load is one in which the load currents have equal magnitudes and phase angles, i.e., $A_{ab,k} = A_{bc,k} = A_{ca,k}$ and $\delta_{ab,k} = \delta_{bc,k} = \delta_{ca,k}$ for every k. The impedances are $Z_{ab} = Z_{bc} = Z_{ca} = Ze^{j\phi}$, where ϕ is the angle of the voltage with respect to the corresponding current (i.e., $\phi = \theta - \delta$). For a balanced load, the relative line current magnitudes are [1, 1, 1]. There is a one-to-one mapping between the power per phase and power per delta phase.

A. BALANCED NONLINEAR LOADS

If the load is nonlinear, i.e., has nonsinusoidal current waveforms, the higher order current harmonics and their relative magnitudes are also of significance. Here, we are focused on loads which may contribute higher order harmonics at multiples of the line frequency, such as power electronic devices. Some loads, such as induction motors, can have "slot harmonics" which are not multiples of the line frequency but are instead related to the slip frequency [29]. However, for the purposes of this article, induction machines without power electronic control are considered approximately linear.

In a balanced delta system, the triplen (e.g., third, sixth, and ninth order) components are zero sequence. The zero-sequence line currents are equal to $(1/3)(i_a + i_b + i_c)$ [30]. Given Kirchoff's current law (KCL) which requires $i_a + i_b + i_c = 0$, the zero-sequence line currents must be zero. That is, they circulate around the delta but do not flow through the lines. The fifth-order harmonics are typically negative sequence, while the seventh-order harmonics are typically positive sequence. Thus, balanced fifth-order and seventh-order line current harmonics are expected.

For example, a variable frequency drive (VFD) is a common nonlinear load used to optimize and control induction motors. A VFD consists of a rectifier, a dc-bus link, and an inverter. The front-end rectifier draws currents rich with harmonic content. A VFD was modeled as shown in Fig. 6, using a constant current source i_{load} to model the inverter-motor combination [31]. The line currents of a simulated 1-kW load controlled by a VFD with a balanced source voltage of $V_{pk} = 170$ V is shown in Fig. 7. The current is characterized by the double pulses of equal magnitude at each positive and negative voltage peak. Fig. 8 shows the mean magnitude for the 5-s simulation of the third, fifth, and seventh harmonic current envelopes, normalized by the magnitude of the fundamental (i.e., $|I_{\psi k}/I_{\psi 1}|$). As expected, the third-order harmonics are negligible. There are significant fifth and seventh-order harmonics, which are balanced among the phases. The relative line current magnitudes can

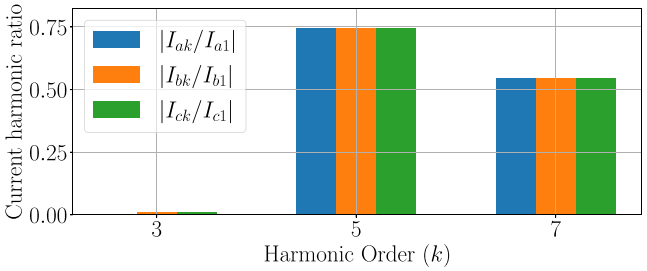

FIGURE 8. Magnitude of third, fifth, and seventh harmonic current envelopes normalized by the fundamental of a motor controlled by VFD.

also be calculated for each relevant harmonic k, which, in this example, is [1, 1, 1] for $k = 5$ and 7.

B. GRADUAL DRIFT OF BALANCED LOADS

A three-phase load can remain balanced while experiencing slow changes in total power due to changing environmental conditions, changing operating conditions, or degradation in condition. Once the load has been identified as being balanced, then the total power can be examined for other subtle changes in load operation, such as slow changes in power consumption due to a soft fault [8]. Identifying slow changes in total power consumption may require either sufficient historical data [10] or an adaptive classifier that can characterize and track gradual load drift [12]. Soft faults, such as loss of refrigerant, slipping belts, and clogged ventilation systems, can leave the system operating at reduced efficiency and induce wear on the system. For instance, a NILM on USCGC SPENCER revealed the slow change in steady-state power of a fuel oil purifier (FOP) centrifuge. Fig. 9(a) shows the relative magnitudes of the FOP centrifuge over a four-year period, where each data point represents a single on-event with $\Delta t = 0.5$ s for steady-state calculation. The relative magnitudes stay approximately constant and balanced for the entire duration. Fig. 9(b) shows the total steady-state power (P_{ss}) of the FOP centrifuge at each on-event, which varies from approximately 10 to 15 kW. This increase in power over time can potentially be attributed to load aging and wear.

V. IMBALANCES IN THREE-PHASE SYSTEMS

Imbalances that occur during transients need to be correctly attributed to healthy or faulty behavior. For a two-phase or single-phase load, the relative current ratios are predictable, as shown in Table 1 for the ideal scenario. Fig. 10 shows the relative magnitudes over time for a single-phase ship service diesel generator (SSDG) lube oil (LO) heater on USCGC SPENCER. Each data point represents a single on-event with $\Delta t = 0.5$ s for steady-state calculation. Here, the measured relative magnitudes for $|I_{a1,ss}/I_{b1,ss}|$, $|I_{b1,ss}/I_{c1,ss}|$, and $|I_{c1,ss}/I_{a1,ss}|$ are generally less than 0.001, 1 ± 0.05, and greater than 1000, respectively. Using a tolerance for allowable divergence from expected values, this matches that of a single-phase load on phase bc. If an event is identified

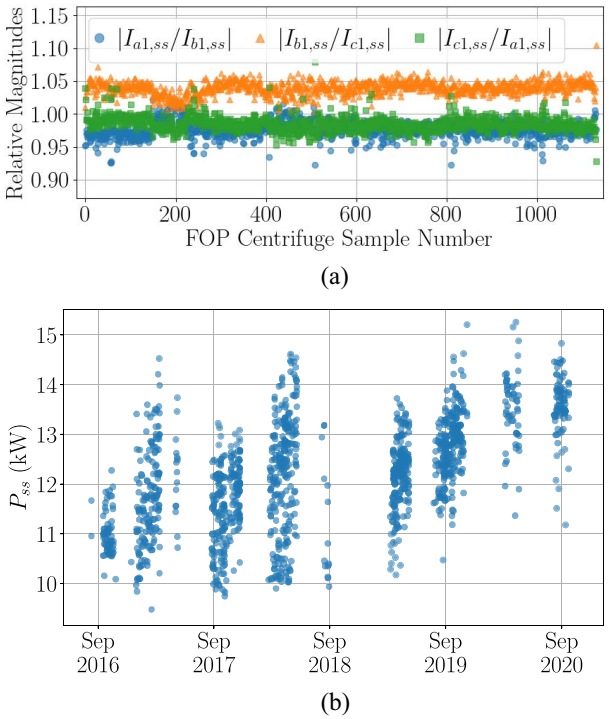

FIGURE 9. Three-phase FOP centrifuge over time: (a) relative line current magnitudes and (b) total steady-state real power (P_{ss}).

TABLE 1. Phase currents based on relative line current magnitudes.

	Relative line current magnitudes			Phase currents		
	$\left\|\frac{I_{a1,ss}}{I_{b1,ss}}\right\|$	$\left\|\frac{I_{b1,ss}}{I_{c1,ss}}\right\|$	$\left\|\frac{I_{c1,ss}}{I_{a1,ss}}\right\|$	i_{ab}	i_{bc}	i_{ca}
Two delta phases	$\sqrt{3}$	1	$\frac{1}{\sqrt{3}}$	$-i_b$	0	i_c
	$\frac{1}{\sqrt{3}}$	$\sqrt{3}$	1	i_a	$-i_c$	0
	1	$\frac{1}{\sqrt{3}}$	$\sqrt{3}$	0	i_b	$-i_a$
Single delta phase	0	1	∞	0	i_b	0
	1	∞	0	i_a	0	0
	∞	0	1	0	0	i_c

as being connected on two delta phases or a single delta phase, then the phase currents can be designated as given in Table 1. The rms spectral envelopes for i_{ab}, i_{bc}, and i_{ca} can be computed with the same process as described in Section II, but with phase rotations of 0°, 120°, and 240°. The power per delta phase can be calculated by multiplying by a constant $\sqrt{3}$ V or by the rms spectral envelopes of the line-to-line voltages. If a step change is detected that does not match the expected relative magnitudes of either a three-phase, two-phase, or single-phase load, then the phase currents cannot be estimated. This provides indication of a possible fault condition. This section presents an analysis of both normal and faulty imbalances.

A. SINGLE-PHASE LOADS

A delta single-phase load inherently imparts an imbalance on the system. For example, the power per phase of a single-phase induction motor from NILM field data is shown in Fig. 11(a). There is an unbalanced amount of P and Q on

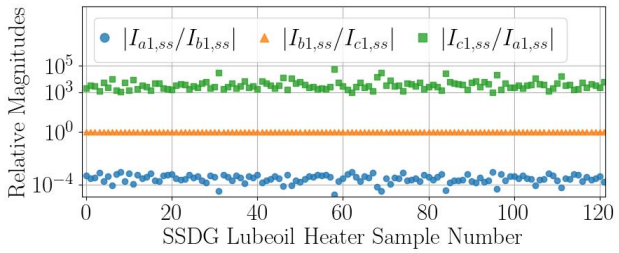

FIGURE 10. Relative magnitudes of single-phase SSDG lubeoil heater load on-events over time.

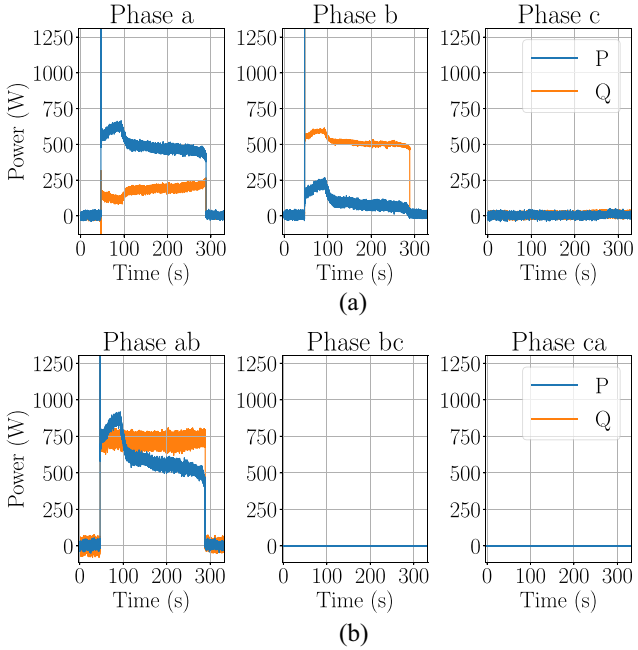

FIGURE 11. (a) Measured power per phase of a single-phase inductive load. (b) Reconstructed power per delta phase.

phases a and b. However, the imbalance here is normal load behavior. The measured relative line current magnitudes for the detected on-event are [1.008, 119.7, 0.008]. These closely match the expected values for a phase ab single-phase load. The phase currents were reconstructed and power per delta phase was computed, as shown in Fig. 11(b). From the delta phase power, it is now possible to track subtle changes over time for this load.

The delta phase power is useful for diagnostics, however, the per-phase power may still prove useful for load identification. The question arises if the imbalances have any physical interpretation? The relationship between the power per delta phase and the power per phase can be determined mathematically. The relationships are shown in Table 2 for a single-phase load on phase ca with impedance $\mathrm{Z_{ca}} = Ze^{j\phi}$. Similar relationships can be derived for single-phase loads on phase ab or bc. The proportion of real and reactive power on phases a and c depends on ϕ. For example, consider a resistive (i.e., $\phi = 0$) load with power on phase ca equal to the load's nominal power P_r, such that $P_{ca} = P_r$ and

TABLE 2. Line-to-line single-phase load relationships.

	Delta phase	Per phase
Currents	$\mathrm{i_{ab}} = 0$ $\mathrm{i_{bc}} = 0$ $\mathrm{i_{ca}} = \sqrt{3}\frac{V}{Z}e^{j(\frac{5\pi}{6}-\phi)}$	$\mathrm{i_a} = -\mathrm{i_{ca}}$ $\mathrm{i_b} = 0$ $\mathrm{i_c} = \mathrm{i_{ca}}$
Real Power	$P_{ab} = 0$ $P_{bc} = 0$ $P_{ca} = 3\frac{V^2}{Z}\cos\phi$	$P_a = \sqrt{3}\frac{V^2}{Z}\cos(\phi + \frac{\pi}{6})$ $P_b = 0$ $P_c = \sqrt{3}\frac{V^2}{Z}\cos(\phi - \frac{\pi}{6})$
Reactive Power	$Q_{ab} = 0$ $Q_{bc} = 0$ $Q_{ca} = 3\frac{V^2}{Z}\sin\phi$	$Q_a = \sqrt{3}\frac{V^2}{Z}\sin(\phi + \frac{\pi}{6})$ $Q_b = 0$ $Q_c = \sqrt{3}\frac{V^2}{Z}\sin(\phi - \frac{\pi}{6})$

$Q_{ca} = 0$. The real power on each phase is: $P_a = P_{ca}/2$, $P_b = 0$, and $P_c = P_{ca}/2$. The reactive power on each phase is: $Q_a = P_{ca}/(2\sqrt{3})$, $Q_b = 0$, and $Q_c = -P_{ca}/(2\sqrt{3})$. That is, due to the imbalance imparted on the system, there is equal magnitude but opposite sign "reactive" power on two of the phases.

This reactive power for a resistive load can be related to the fact that standard definitions of reactive and apparent power are unable to simultaneously characterize the efficiency of equipment, efficiency of power transmission, and oscillatory character of power transfer in unbalanced and polyphase systems [16], [17]. Definitions which use different assumptions about the system can provide possible additional features. For instance, the arithmetic apparent power is the arithmetic sum of the apparent power of the individual phases, $S_A = \sum_\psi \sqrt{P_\psi^2 + Q_\psi^2}$ [17]. The vector apparent power is the magnitude of the total vector power, $S_V = \sqrt{(\sum_\psi P_\psi)^2 + (\sum_\psi Q_\psi)^2}$ [17]. The arithmetic and vector power factors are $\mathrm{PF}_A = P_{\mathrm{total}}/S_A$ and $\mathrm{PF}_V = P_{\mathrm{total}}/S_V$. For a resistive single-phase load $\mathrm{PF}_A = 0.866$ and $\mathrm{PF}_V = 1.0$. The arithmetic power factor is less than one, which is a result of the per phase reactive power. The power per phase and the arithmetic power factor both take into account imbalances imparted on the system, and can provide a unique load signature for load identification. However, the delta phase power and vector power factor are more intuitive diagnostic metrics for reporting load behavior. The vector power factor represents the individual load's power factor, without consideration for any imbalances imparted on the system. That is, it physically makes sense for a resistive load to have a power factor close to one.

B. THREE-PHASE HEATER FAULTS

A delta-connected resistive or heating load consists of three heating elements connected line-to-line. This type of load can experience numerous failures due to the degradation of materials in industrial environments. Fig. 12 shows two examples of degradation pertaining to a three-phase heater from two different USCG shipboard microgrids. Specifically, Fig. 12(a) shows deteriorated heating elements and Fig. 12(b) shows a loose connection and degraded cable insulation. These faults result in various electrical failure signatures.

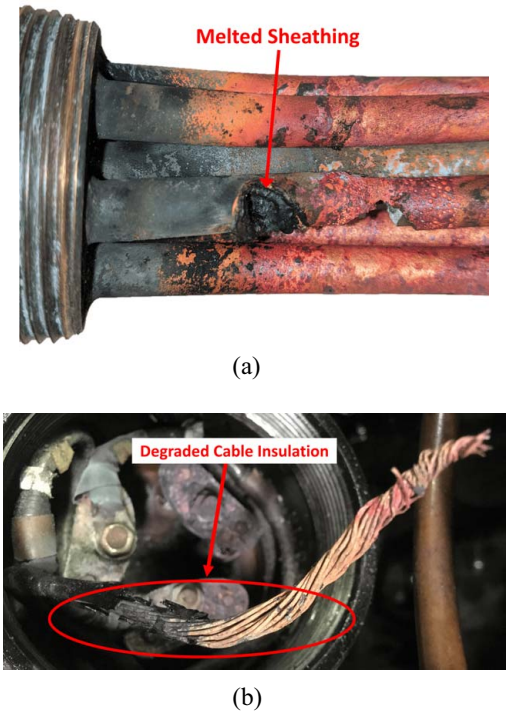

FIGURE 12. Two degraded three-phase heaters: (a) significant corrosion and melted sheathing of heating elements [13] and (b) loose wire connection and degraded cable insulation.

TABLE 3. Line-to line open circuit fault relationships.

	Delta phase	Per phase
Currents	$\mathrm{i}_{\mathrm{ab}} = 0$ $\mathrm{i}_{\mathrm{bc}} = \sqrt{3}\frac{V}{Z}e^{j(-\frac{\pi}{2}-\phi)}$ $\mathrm{i}_{\mathrm{ca}} = \sqrt{3}\frac{V}{Z}e^{j(\frac{5\pi}{6}-\phi)}$	$\mathrm{i}_{\mathrm{a}} = -\mathrm{i}_{\mathrm{ca}}$ $\mathrm{i}_{\mathrm{b}} = \mathrm{i}_{\mathrm{bc}}$ $\mathrm{i}_{\mathrm{c}} = 3\frac{V}{Z}e^{j(\frac{2\pi}{3}-\phi)}$
Real Power	$P_{ab} = 0$ $P_{bc} = 3\frac{V^2}{Z}\cos\phi$ $P_{ca} = 3\frac{V^2}{Z}\cos\phi$	$P_a = \sqrt{3}\frac{V^2}{Z}\cos(\phi+\frac{\pi}{6})$ $P_b = \sqrt{3}\frac{V^2}{Z}\cos(\phi-\frac{\pi}{6})$ $P_c = 3\frac{V^2}{Z}\cos\phi$
Reactive Power	$Q_{ab} = 0$ $Q_{bc} = 3\frac{V^2}{Z}\sin\phi$ $Q_{ca} = 3\frac{V^2}{Z}\sin\phi$	$Q_a = \sqrt{3}\frac{V^2}{Z}\sin(\phi+\frac{\pi}{6})$ $Q_b = \sqrt{3}\frac{V^2}{Z}\sin(\phi-\frac{\pi}{6})$ $Q_c = 3\frac{V^2}{Z}\sin\phi$

The first fault condition considered is a line-to-line open circuit. This can result from a failed heating element, for example due to damaged sheathing and corrosion. A line-to-line open circuit manifests as a reduction in magnitude and phase shift in two of the line currents. That is, the three-phase load acts as a two-phase load. Given a phase *ab* open circuit such that $Z_{ab} = \infty$, $Z_{bc} = Ze^{j\phi}$, and $Z_{ca} = Ze^{j\phi}$, Table 3 presents the relationship between the power per delta phase and the power per phase. Similar relationships can be derived for a *bc* or *ca* open circuit. If there is a second line-to-line open circuit, it would act as a single-phase load. Fig. 13 shows the power for a simulated 3-kW resistive load with a phase *ab* open circuit. Fig. 13(a) shows the power as calculated from the line currents. The phase currents are reconstructed and power per delta phase is computed, as shown in Fig. 13(b). The power per delta phase correctly shows 1 kW on both phases *bc* and *ca*. The next fault condition considered is a missing voltage connection to the load,

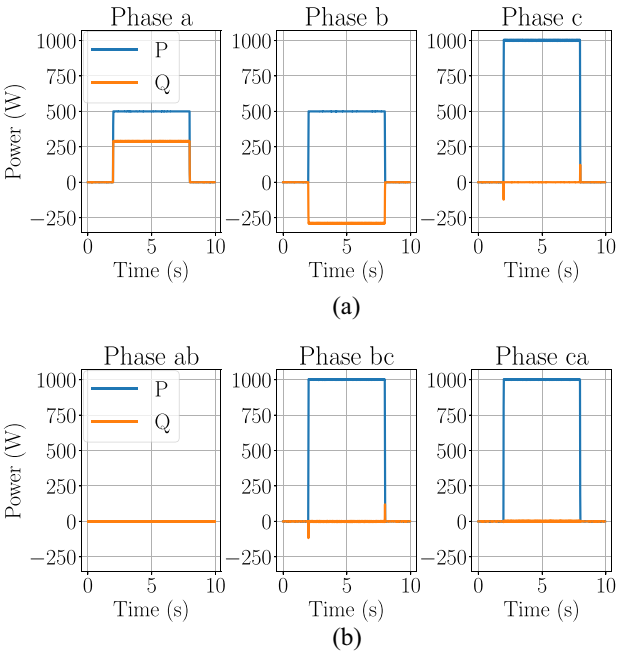

FIGURE 13. (a) Per-phase power of a two-phase resistive load. (b) Reconstructed power per delta phase.

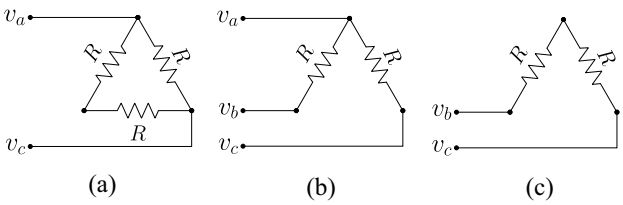

FIGURE 14. Delta-connected heater under various fault conditions: (a) missing voltage v_b connection, (b) phase *bc* open circuit, and (c) both a missing voltage v_a connection and phase *bc* open circuit.

essentially turning a three-phase load into a single-phase load. This can result from degraded or loose wiring in the terminal box. Fig. 14 shows conceptual diagrams for examples of these two fault scenarios (line-to-line open-circuit and missing voltage connection), plus the combination of both faults simultaneously. Here, R is the resistance of a single heating element. Table 4 shows the resulting delta impedances, delta phase power, per-phase power, and total power for these three fault scenarios for a heating load with nominal rating $P_r = 9(V^2/R)$. With a missing voltage connection, the heater draws one-half of its nominal power. With an open-circuited heating element, the heater draws two-thirds of its nominal power. These two faults combined, depending on which voltage is missing and which heating element is open-circuited, results in the heater drawing either one-sixth [the scenario shown in Fig. 14(c)] or one-third of its nominal power. The heater will also draw one-third of its nominal power if it has two open-circuited heating elements.

These fault scenarios have been observed with NILMs on various USCG shipboard microgrids. Fig. 15 shows the measured per-phase power streams of the nominal 12-kW main propulsion diesel engine (MPDE) jacket water (JW)

TABLE 4. Delta-connected heating load fault conditions.

Delta impedances	Delta phase power	Per phase power		Total power
No v_b connection				
$\mathrm{Z_{ca}} = \frac{2}{3}R$	$P_{ca} = \frac{1}{2}P_r$	$P_a = \frac{1}{4}P_r$ $P_c = \frac{1}{4}P_r$	$Q_a = \frac{1}{4\sqrt{3}}P_r$ $Q_c = -\frac{1}{4\sqrt{3}}P_r$	$\frac{1}{2}P_r$
Phase bc open circuit				
$\mathrm{Z_{ab}} = R$ $\mathrm{Z_{bc}} = \infty$ $\mathrm{Z_{ca}} = R$	$P_{ab} = \frac{1}{3}P_r$ $P_{bc} = 0$ $P_{ca} = \frac{1}{3}P_r$	$P_a = \frac{1}{3}P_r$ $P_b = \frac{1}{6}P_r$ $P_c = \frac{1}{6}P_r$	$Q_a = 0$ $Q_b = \frac{1}{6\sqrt{3}}P_r$ $Q_c = -\frac{1}{6\sqrt{3}}P_r$	$\frac{2}{3}P_r$
Phase bc open circuit and no v_a connection				
$\mathrm{Z_{bc}} = 2R$	$P_{bc} = \frac{1}{6}P_r$	$P_b = \frac{1}{12}P_r$ $P_c = \frac{1}{12}P_r$	$Q_b = -\frac{1}{12\sqrt{3}}P_r$ $Q_c = \frac{1}{12\sqrt{3}}P_r$	$\frac{1}{6}P_r$

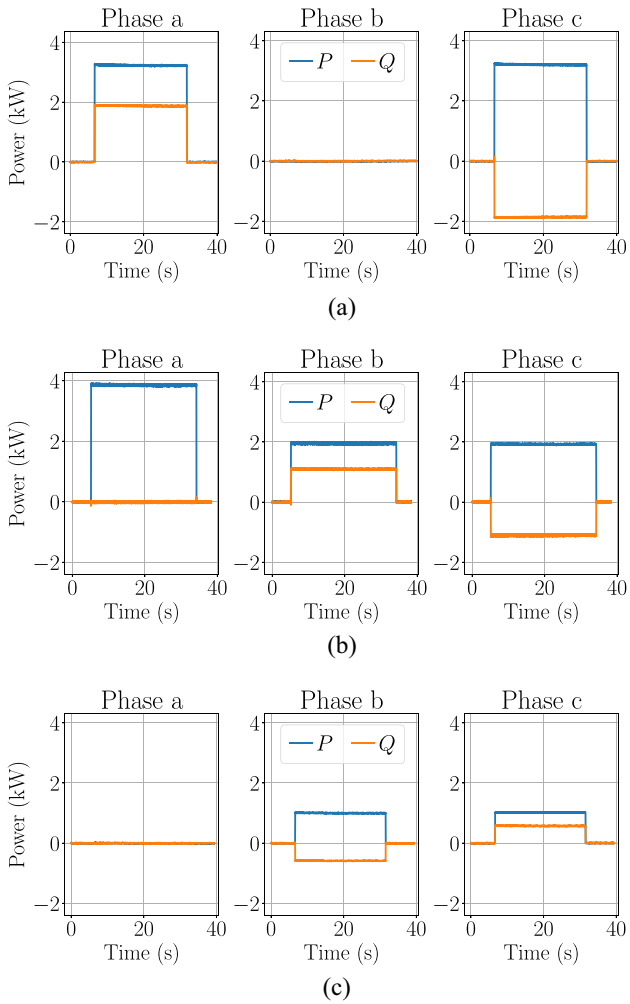

FIGURE 15. Per-phase *P* and *Q* for MPDE JW heater in various fault scenarios: (a) port-side heater with a missing voltage connection, (b) stbd-side heater with a line-to-line open circuit, and (c) stbd-side heater with a line-to-line open circuit and a missing voltage connection.

heater on USCGC THUNDER BAY in these various fault states. The baseline power has been subtracted out for easier visual display. The port-side MPDE JW heater in Fig. 15(a) is drawing a total of 6 kW, due to a missing v_b voltage connection. It appears as a single-phase load in this faulty state, with measured relative line current magnitudes, [653.54, 0.0015, 0.9913]. This matches that of a phase *ca* single-phase load. The starboard-side MPDE JW heater in Fig. 15(b) is drawing 8 kW. This is due to an open circuited phase *bc* heating element. The relative line current magnitudes for this load, [1.7315, 0.9995, 0.5778], match that of a two-phase load on phases *ab* and *ca*. This heater previously had no v_a voltage connection due to corroded wiring, as shown in Fig. 12(b). Combined with the line-to-line open circuit, the heater was only drawing 2 kW, as shown in Fig. 15(c). The measured relative current magnitudes in this state, [0.0004, 0.9977, 239.92], matches that of a phase *bc* single-phase load. The per-phase power for these three scenarios matches the expected values from Table 4.

These events are difficult for ship personnel to detect, as the heater uses its operational heating element(s) to still warm the JW. Only after three heating elements open circuit or two loose voltage connections will the heating system have a complete system failure. Thermostat-based controllers driving these heaters alter run times to ensure JW temperatures are regulated. Only in the extremely degraded state of Fig. 15(c) was the heater not able to produce the heat output necessary, even when the heater was operating with an approximately 100% duty cycle. These failures indicate that the heater may be at risk for other damaging failures with potentially dangerous operating conditions. Thus, the degraded heater should be detected as early as possible. However, these events are difficult for a pattern classifier to detect if only trained on healthy load data. As was shown, these failure signatures are predictable. Thus, a NILM pattern classifier can be trained to recognize these failure events using simulated degraded load transients. These presented three-phase heater faults are examples of complete degradation of part of the system (e.g., a resistance goes to open-circuit). However, it is possible for the degradation of the heating element to result in only partial failure (e.g., the resistance increases or decreases in value). In such cases, it would likely be possible to use the adaptive classifier techniques demonstrated in [12] to track the gradual changes in steady-state power and relative line current magnitudes.

C. HIGH CURRENT ARCING FAULT

Degraded materials can lead to damaged sheathing or exposed wiring and can cause arcing or direct shorting between the phases. Standard protection for high-current arcing includes circuit-breakers. The amount of time required for a circuit breaker to trip at a specific current magnitude is based on the breaker's time-current curve. Two arcing events were observed on USCGC SPENCER, as also detailed in [13]. These arcing events are attributed to the degradation of the copper sheathing of a 4.5-kW MPDE JW heater, since the currents return to normal levels with the turn-off of the heater. Both events clipped at the 300-A limit of the NILM current sensors. The currents of the first event are shown in Fig. 16. The arcing event lasted for about six line cycles and occurred while the heater was drawing the nominal 4.5 kW. All three phases experience a large current spike. Using curve fitting on the clipped current data to estimate

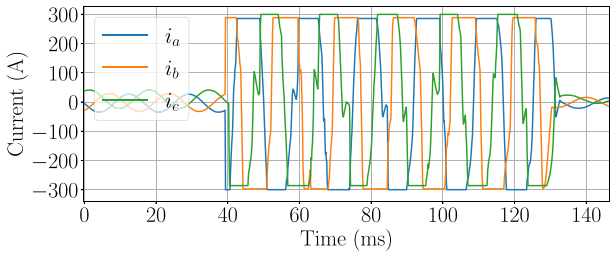

FIGURE 16. Currents during the first arcing event, in which all three line currents spike [13].

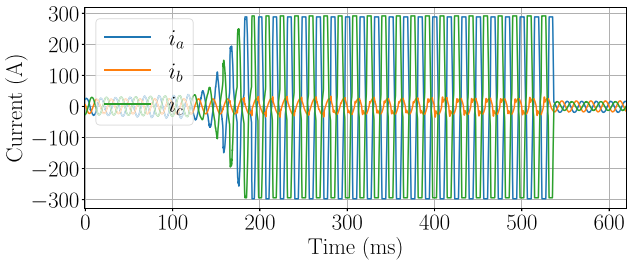

FIGURE 17. Currents during the second arcing event, in which phases *a* and *c* show current spikes.

the true current magnitude, it was estimated that the current on phase b was greater than that of phases a and c. The second arcing event occurred approximately 9-h later. In the interval between these arcing events, two heating elements open circuited. Thus, during the second arcing event only the ca element is operating and only phases c and a experience spikes in current. This event lasted for about 22 line cycles, as shown in Fig. 17.

The heater is supplied from a 15-A breaker with an instantaneous trip rating of 180–750-A rms. The ship personnel reported that they had no indication that these arcing events occurred or of any breakers having tripped. From curve fitting on the clipped current data, it was estimated that both events fell between the breaker's minimum and maximum clearing times. An exact magnitude cannot be determined because of the clipping and distortions around the zero-crossing, but the estimates indicate that the arcs may have self-extinguished prior to tripping the breakers. The standard protection and relaying on this power system failed to catch the dangerous arcing that was clearly observable in the electrical streams. A NILM can alert watchstanders to any unusually high power events as indication of arcing. Removal of the heater after the arcing event in Fig. 17 revealed significant damage, as shown in Fig. 12(a).

D. HIGH IMPEDANCE GROUND FAULT

As described in [13], the sheathing of the MPDE JW heaters installed on the USCG cutters are grounded. Damage to the sheathing and heating elements may lead to a ground fault. It is critical to detect and locate any ground faults for power utilization safety. The monitored shipboard systems are nominally ungrounded systems. However, an ungrounded

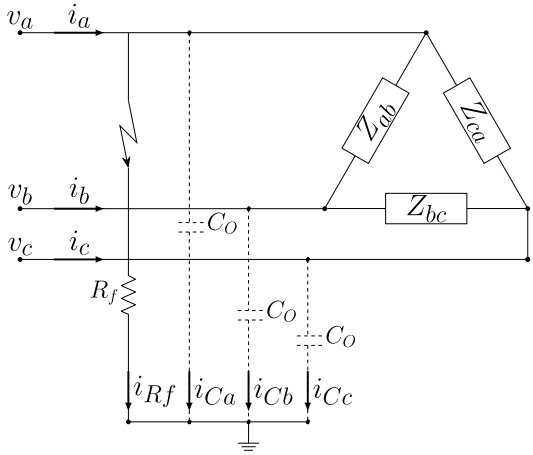

FIGURE 18. Ungrounded power system with a phase-*a* fault to ground. The system is parasitically grounded through the capacitances between the three-phase conductors and ground.

system is in reality capacitively grounded through the parasitic, or natural capacitances of three-phase conductors and other distribution equipment to ground (e.g., the ship's hull). This creates an inherent capacitive current [32]. The capacitive impedances of ungrounded systems limits the ground fault current and makes them "high-impedance faults." As a result, these faults may be similar in magnitude to those of normal loads [33], [34]. In these cases, detection of a ground fault is often performed with a zero-sequence voltage relay. Locating ground faults requires the manual sequential opening of branch circuits until the fault disappears [33]. As will be described, a ground fault manifests as a unique power signature. This enables the use of a NILM to detect ground faults and supplement existing protection schemes.

Fig. 18 shows a diagram for an ungrounded power system with parasitic capacitances C_0 between each phase and ground, and a phase-a fault to ground. For an unfaulted scenario and assuming balanced voltages as given in (2), the capacitive currents are

$$\begin{bmatrix} i_{Ca} \\ i_{Cb} \\ i_{Cc} \end{bmatrix} = \begin{bmatrix} \omega C_0 V e^{j\frac{\pi}{2}} \\ \omega C_0 V e^{-j\frac{\pi}{6}} \\ \omega C_0 V e^{-j\frac{5\pi}{6}} \end{bmatrix}. \tag{10}$$

The parasitic capacitances are the only current return path during a ground fault. Given a phase-a solid ground fault, the line-to-ground voltages and capacitive currents are

$$\begin{bmatrix} v_{ag} \\ v_{bg} \\ v_{cg} \end{bmatrix} = \begin{bmatrix} 0 \\ \sqrt{3} V e^{-j\frac{5\pi}{6}} \\ \sqrt{3} V e^{j\frac{5\pi}{6}} \end{bmatrix}, \quad \begin{bmatrix} i_{Ca} \\ i_{Cb} \\ i_{Cc} \end{bmatrix} = \begin{bmatrix} 0 \\ \sqrt{3}\omega C_0 V e^{-j\frac{\pi}{3}} \\ \sqrt{3}\omega C_0 V e^{-j\frac{2\pi}{3}} \end{bmatrix}. \tag{11}$$

In this case, the faulted phase and ground potential are equated and the voltage of the two unfaulted phases to ground are raised from V to $\sqrt{3}\ V$ [32]. The line-to-line voltages do not change with a ground fault. That is, a single line-to-ground fault does not cause any service disruptions.

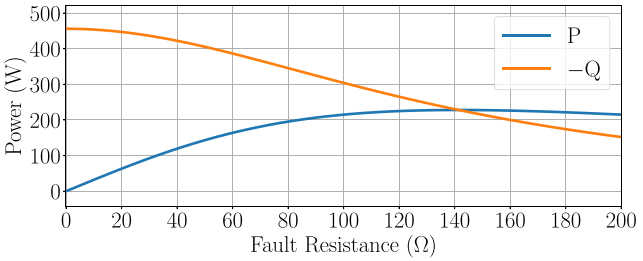

FIGURE 19. Ground fault power on the faulted phase for different fault resistances.

Instead, a shifting of the neutral occurs. Using KCL, the fault current is three times the original capacitive current from each phase to ground. Ground faults often occur with some resistance, R_f, associated with the fault, which affects the line-to-ground voltage shift and fault current magnitude. Ignoring line impedances, the line-to-ground voltage for a phase-a fault to ground is

$$\mathrm{v_{ag}} = \mathrm{V}\frac{j3\omega C_0 R_f}{1 + j3\omega C_0 R_f}. \tag{12}$$

The total phase-a fault current is

$$\mathrm{i_{fault}} = j3\omega C_0 \mathrm{V}\frac{1 + j\omega C_0 R_f}{1 + j3\omega C_0 R_f}. \tag{13}$$

The proportion of the fault current that gets measured in the line current of the faulted phase is the current through the fault resistance, which can be solved for by current division

$$\mathrm{i_{R_f}} = \frac{j3\omega C_0 \mathrm{V}}{1 + j3\omega C_0 R_f}. \tag{14}$$

If R_f is zero, the current as measured by the NILM is three times the original capacitive current from each phase to ground. As R_f increases, the change in line-to-ground voltage decreases and the fault current decreases. In terms of power [using the definition in (6) which assumes a constant voltage, V], if R_f is zero, a negative Q will be added to the aggregate power stream. If R_f is nonzero, the ground fault also adds a positive P to the faulted phase. For example, with a parasitic capacitance $C_0 = 6.25\ \mu$F, P and Q as would be measured by a NILM on the faulted phase for fault resistances ranging from 0 to 200 Ω is shown in Fig. 19.

Two line-to-ground fault events were observed on USCGC SPENCER. These events may have been due to the damaged sheathing and degraded heating elements of the MPDE JW heaters. Fig. 20(a) shows the aggregate power during the first ground fault, which was also presented in [13]. There is a ground fault on phase-c at $t = 0.6$ min, appearing as a step change in P_c and Q_c of approximately 109 W and −437 VAR, respectively. There is no significant change in power on the other two phases. The relative line current magnitudes for this observed fault are [2.462, 0.005, 74.060], which do not match any of the expected values. A similar ground fault was observed several months later on phase-b, as shown in Fig. 21(a). At $t = 0.35$ min, there is a step change in P_b and Q_b of approximately 88 W and −448 VAR, respectively. Similar to the first ground fault, there is no significant change

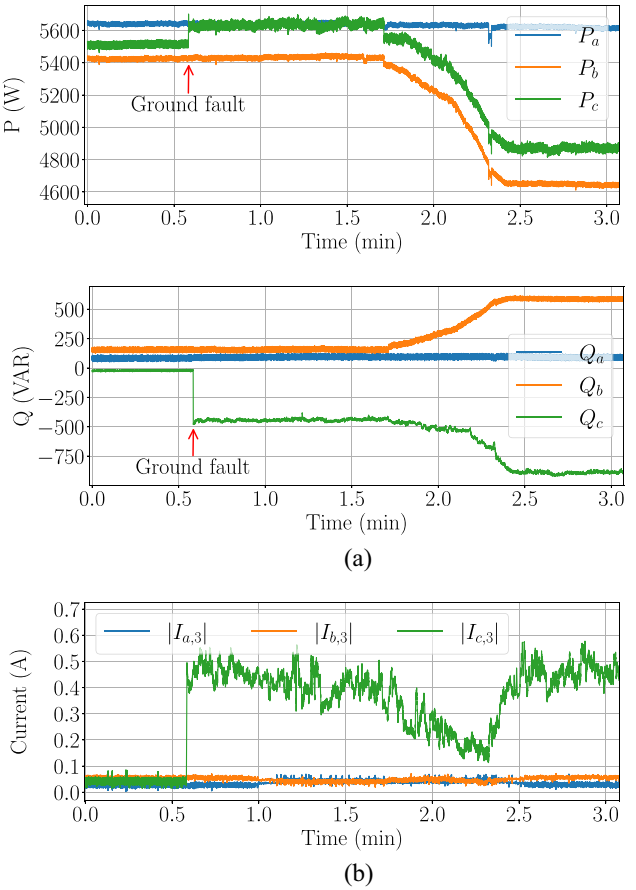

FIGURE 20. (a) Aggregate real and reactive power with a phase-*c* ground fault at 0.6 min immediately followed by an open circuit of the *bc* heating element. (b) Third harmonic current during the ground fault [13].

in power on the two healthy phases. The relative current magnitudes of this ground fault are [0.003, 34.334, 9.343]. A ground fault also leads to third-harmonic line current in the faulted phase [34]. As mentioned, third-harmonic currents are typically zero-sequence components. With a ground fault, a low impedance path is provided for the zero-sequence components. Figs. 20(b) and 21(b) show the rms third-harmonic current envelopes for the two ground faults, with a 12-point rolling mean applied.

The nature of the high-impedance ground fault has meaningful implications for using a NILM to detect these faults. Even though the step change in power is similar in magnitude to those of normal loads, the way it manifests as increased line currents on only a single phase, both fundamental and third-harmonic, is likely unique. All the load connection types described have line currents on at least two of the lines. The relative line current magnitudes can also provide an indication of a ground fault. The relative line current magnitudes for a ground fault will contain a 0 and ∞ (realistically just a large value), similar to a single-phase load. The third value depends on the step changes of the line currents of the two healthy phases, which are both close to 0, so it is unlikely for the ratio to be exactly 1. If the ground fault is due to faulty load behavior, the location can

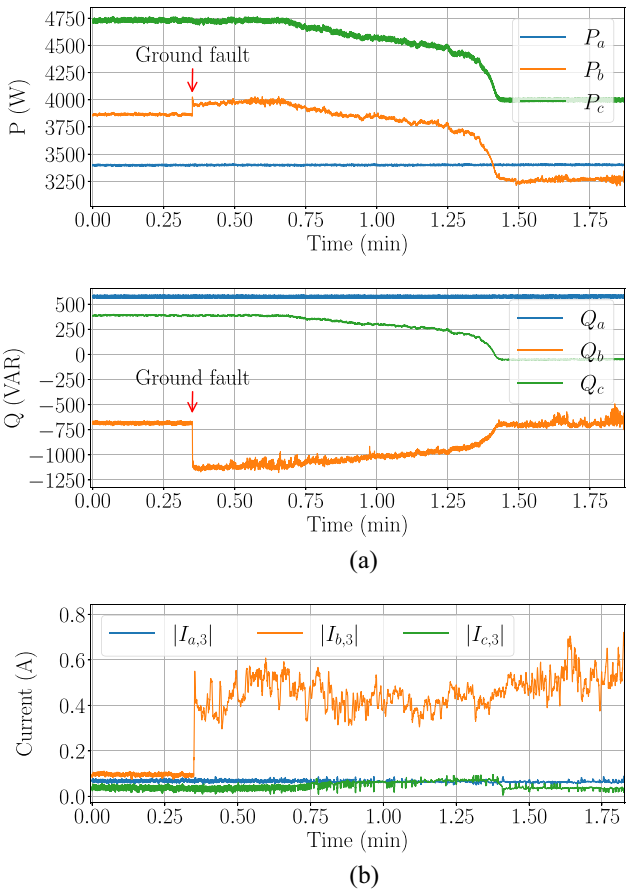

FIGURE 21. (a) Aggregate real and reactive power with a phase-*b* ground fault at 0.35 min immediately followed by an open circuit of the *bc* heating element. (b) Third harmonic current during the ground fault.

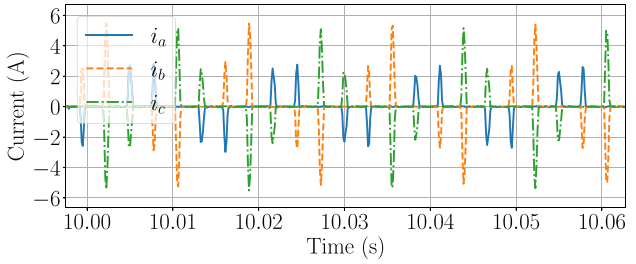

FIGURE 22. Unbalanced line currents for a motor controlled by a VFD.

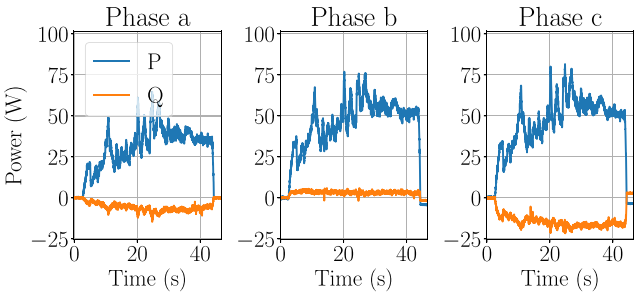

FIGURE 23. Power envelopes of a motor controlled by a VFD.

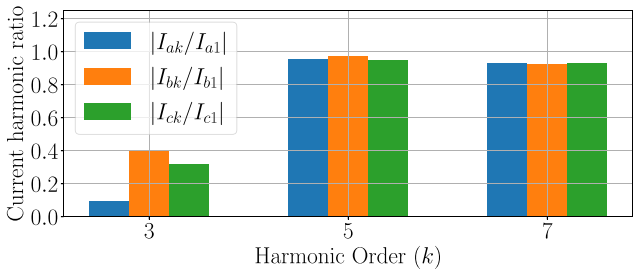

FIGURE 24. Magnitude of third, fifth, and seventh harmonic current envelopes normalized by the fundamental of a motor controlled by a VFD.

be narrowed down to the energized equipment as identified by a NILM classifier.

These ground faults were both immediately followed by the open circuit of a *bc* heating element of a MPDE JW heater. As shown in Figs. 20(a), and 21(a) the ground faults were followed by a slow change in power until about $t = 2.4$ min and $t = 1.4$ min, respectively, as a result of the open circuit. This heater is nominally 4.5 kW, so as expected, the open circuited heating elements result in a decrease of about 750 W on phases *b* and *c*, and a split of about 433 VAR on those phases.

E. UNBALANCED NONLINEAR LOADS

For calculating per-phase power, ideally balanced and sinusoidal voltages have been assumed. However, it is also important to consider the imbalances in the measured line-to-line voltages. Unbalanced supply voltages may be especially prevalent on some systems such as on marine microgrids [35] and on grids with high penetration of distributed energy resources such as photovoltaics [36]. For a VFD, even small voltage imbalances can cause significant variation in line current waveforms [37]. As the voltage imbalance increases, the same amount of power still needs to be supplied, resulting in current peak increases. This means an increased current through the diodes and increased stress on the components. With a large enough supply voltage imbalance, the balanced double-pulse line current waveform eventually becomes a single pulse waveform. As described in Section IV, for a balanced nonlinear load, triplen components are zero-sequence. More generally, the third harmonic line currents are

$$\begin{aligned} i_{a3}(t) &= A_{ab3}\cos(3\omega t + \delta_{ab3}) - A_{ca3}\cos(3\omega t + \delta_{ca3}) \\ i_{b3}(t) &= A_{bc3}\cos(3\omega t + \delta_{bc3}) - A_{ab3}\cos(3\omega t + \delta_{ab3}) \\ i_{c3}(t) &= A_{ca3}\cos(3\omega t + \delta_{ca3}) - A_{bc3}\cos(3\omega t + \delta_{bc3}). \end{aligned} \quad (15)$$

When the third harmonic phase current magnitudes and phase angles are not equal, third harmonic line currents will be measured. That is, the uneven current distribution in the rectifier can cause uncharacteristic positive-sequence triplen harmonics in the line currents [38], [39].

A three-phase motor controlled by a VFD was tested using the laboratory grid voltage. The line currents and per-phase power are shown in Figs. 22 and 23, respectively. The line-to-line voltages during the testing period averaged $V_{ab} = 292.3$ V, $V_{bc} = 295.6$ V, and $V_{ca} = 295.5$ V. Even these small voltage imbalances resulted in an asymmetric current conduction. Fig. 24 shows the average current

TABLE 5. Relative line current magnitudes of unbalanced VFD.

	$\left\lvert\frac{I_{ak,ss}}{I_{bk,ss}}\right\rvert$	$\left\lvert\frac{I_{bk,ss}}{I_{ck,ss}}\right\rvert$	$\left\lvert\frac{I_{ck,ss}}{I_{ak,ss}}\right\rvert$
k=1	0.84	0.91	1.30
k=3	0.36	1.34	2.07
k=5	0.86	0.93	1.25
k=7	0.83	0.93	1.29

harmonic magnitudes normalized by the fundamental for the load duration shown in Fig. 23. Unlike the balanced case of Fig. 8, there are significant third harmonic line currents. The unbalanced line currents also result in relative line current magnitudes that deviate from the expected values of [1, 1, 1], as shown in Table 5 for the fundamental, third, fifth, and seventh harmonics. These values were calculated at the detected on-event with $\Delta t = 1$ s for steady-state calculation. Since the line currents are not balanced, the true phase currents cannot be determined. However, the imbalanced line currents and presence of third harmonic currents are a telling sign of increased stress on components and possible power quality issues.

VI. CONCLUSION

Load identification and condition monitoring with nonintrusive load monitoring relies on the correct physical interpretation of measurements. As was demonstrated, faults are associated with changing electrical consumption and often evolve in a predictable way. Electrical analysis unveiled degraded shipboard loads, revealing corrosion and degradation of critical equipment. Monitoring these systems is important for ensuring efficient and safe operation. A practical three-phase system is never perfectly balanced. Changes in system balances for currents, voltages, and harmonic content during transients can inform load identification and diagnostics. Nonintrusive load monitoring can be used as a condition-based maintenance aid, by using power stream data to detect load or system degradation before complete failure occurs.

ACKNOWLEDGMENT

The authors gratefully acknowledge the U.S. Coast Guard and in particular the crews of USCGC SPENCER and USCGC THUNDER BAY for granting access to their ships.

REFERENCES

[1] G. Xu, M. Liu, Z. Jiang, W. Shen, and C. Huang, "Online fault diagnosis method based on transfer convolutional neural networks," *IEEE Trans. Instrum. Meas.*, vol. 69, no. 2, pp. 509–520, Feb. 2020.

[2] B. Gustavsen, M. Häyer-Hansen, M. Hatlo, and S. Midttveit, "Voltages and AC corrosion on metallic tubes in umbilical cables caused by magnetic induction from power cable charging currents," *IEEE Trans. Power Del.*, vol. 34, no. 2, pp. 596–605, Apr. 2019.

[3] S. Samarasinghe *et al.*, "A risk assessment for utilities to prevent transformer OLTC failures caused by silver sulphide corrosion," *IEEE Trans. Power Del.*, vol. 37, no. 3, pp. 2394–2402, Jun. 2022.

[4] J. Paris, J. S. Donnal, and S. B. Leeb, "NilmDB: The non-intrusive load monitor database," *IEEE Trans. Smart Grid*, vol. 5, no. 5, pp. 2459–2467, Sep. 2014.

[5] H. Hwang and S. Kang, "Nonintrusive load monitoring using an LSTM with feedback structure," *IEEE Trans. Instrum. Meas.*, vol. 71, pp. 1–11, 2022.

[6] G. Karniadakis, Y. Kevrekidis, L. Lu, P. Perdikaris, S. Wang, and L. Yang, "Physics-informed machine learning," *Nat. Rev. Phys.*, vol. 3, pp. 422–440, Jun. 2021.

[7] K. Li, J. Liu, Z. Wang, and B. Wei, "Strategies and operating point optimization of STATCOM control for voltage unbalance mitigation in three-phase three-wire systems," *IEEE Trans. Power Del.*, vol. 22, no. 1, pp. 413–422, Jan. 2007.

[8] J. Paris, J. S. Donnal, R. Cox, and S. Leeb, "Hunting cyclic energy wasters," *IEEE Trans. Smart Grid*, vol. 5, no. 6, pp. 2777–2786, Nov. 2014.

[9] P. A. Lindahl, D. H. Green, G. Bredariol, A. Aboulian, J. S. Donnal, and S. B. Leeb, "Shipboard fault detection through Nonintrusive load monitoring: A case study," *IEEE Sensors J.*, vol. 18, no. 21, pp. 8986–8995, Nov. 2018.

[10] A. Aboulian *et al.*, "NILM dashboard: A power system monitor for electromechanical equipment diagnostics," *IEEE Trans. Ind. Informat.*, vol. 15, no. 3, pp. 1405–1414, Mar. 2019.

[11] D. Green, T. Kane, S. Kidwell, P. Lindahl, J. Donnal, and S. Leeb, "NILM dashboard: Actionable feedback for condition-based maintenance," *IEEE Instrum. Meas. Mag.*, vol. 23, no. 5, pp. 3–10, Aug. 2020.

[12] D. H. Green, A. W. Langham, R. A. Agustin, D. W. Quinn, and S. B. Leeb, "Adaptation for automated drift detection in electromechanical machine monitoring," *IEEE Trans. Neural Netw. Learn. Syst.*, early access, Jun. 23, 2022, doi: 10.1109/TNNLS.2022.3184011.

[13] D. H. Green, D. W. Quinn, S. Madden, P. A. Lindahl, and S. B. Leeb, "Nonintrusive measurements for detecting progressive equipment faults," *IEEE Trans. Instrum. Meas.*, vol. 71, pp. 1–12, 2022.

[14] *UE9 Datasheet*, Labjack Corporat., Lakewood, CO, USA, 2020.

[15] H. Akagi, E. H. Watanabe, and M. Aredes, *Instantaneous Power Theory and Applications to Power Conditioning*. Hoboken, NJ, UAS: Wiley, 2007.

[16] J. Willems, "Reflections on apparent power and power factor in nonsinusoidal and polyphase situations," *IEEE Trans. Power Del.*, vol. 19, no. 2, pp. 835–840, Apr. 2004.

[17] *IEEE Standard Definitions for the Measurement of Electric Power Quantities Under Sinusoidal, Nonsinusoidal, Balanced, or Unbalanced Conditions*, IEEE Standard 1459-2010, 2010.

[18] W. G. Morsi and M. E. El-Hawary, "Defining power components in nonsinusoidal unbalanced polyphase systems: The issues," *IEEE Trans. Power Del.*, vol. 22, no. 4, pp. 2428–2438, Oct. 2007.

[19] V. P. Brasil, J. Y. Ishihara, and A. De L. Ferreira Filho, "Fair power factor billing under unbalanced and nonsinusoidal voltage supply," *IEEE Access*, vol. 10, pp. 19301–19311, 2022.

[20] P. C. Krause, O. Wasynczuk, S. D. Sudhoff, and S. Pekarek, *Analysis of Electric Machinery and Drive Systems*. Hoboken, NJ, USA: Wiley, 2013.

[21] J. C. Das, *Understanding Symmetrical Components for Power System Modeling*. Hoboken, NJ, USA: Wiley, 2017.

[22] J. L. Kirtley, *Electric Power Principles*. Hoboken, NJ, USA: Wiley, 2010.

[23] J. Belikov and Y. Levron, "Uses and misuses of quasi-static time-varying phasor models in power systems," *IEEE Trans. Power Del.*, vol. 33, no. 6, pp. 3263–3266, Dec. 2018.

[24] J. Paris, J. Donnal, Z. Remscrim, S. Leeb, and S. Shaw, "The Sinefit spectral envelope preprocessor," *IEEE Sensors J.*, vol. 14, no. 12, pp. 4385–4394, Dec. 2014.

[25] A. W. Langham, D. H. Green, and S. B. Leeb, "Resolution analysis for power system measurement and transient identification," *IEEE Trans. Instrum. Meas.*, vol. 71, pp. 1–10, 2022.

[26] S. B. Leeb, S. R. Shaw, and J. L. Kirtley, "Transient event detection in spectral envelope estimates for nonintrusive load monitoring," *IEEE Trans. Power Del.*, vol. 10, no. 3, pp. 1200–1210, Jul. 1995.

[27] R. Jain, R. Kasturi, and B. G. Schunck, *Machine Vision*. New York, NY, USA: McGraw-Hill, 1995.

[28] D. H. Green, S. R. Shaw, P. Lindahl, T. J. Kane, J. S. Donnal, and S. B. Leeb, "A multiscale framework for nonintrusive load identification," *IEEE Trans. Ind. Informat.*, vol. 16, no. 2, pp. 992–1002, Feb. 2020.

[29] O. Keysan and H. B. Ertan, "Real-time speed and position estimation using rotor slot harmonics," *IEEE Trans. Ind. Informat.*, vol. 9, no. 2, pp. 899–908, May 2013.
[30] D. P. Kothari and I. J. Nagrath, *Modern Power System Analysis*. New York, NY, USA: Tata McGraw-Hill, 2008.
[31] W. Wichakool, A.-T. Avestruz, R. W. Cox, and S. B. Leeb, "Modeling and estimating current harmonics of variable electronic loads," *IEEE Trans. Power Electron.*, vol. 24, no. 12, pp. 2803–2811, Dec. 2009.
[32] D. Paul, "Phase-ground fault current analysis and protection of a high-resistance grounded power system," *IEEE Trans. Ind. Appl.*, vol. 56, no. 4, pp. 3306–3314, Jul./Aug. 2020.
[33] T. Baldwin and F. Renovich, "Analysis of fault locating signals for high-impedance grounded systems," *IEEE Trans. Ind. Appl.*, vol. 38, no. 3, pp. 810–817, May/Jun. 2002.
[34] U. Orji *et al.*, "Adaptive zonal protection for ring microgrids," *IEEE Trans. Smart Grid*, vol. 8, no. 4, pp. 1843–1851, Jul. 2017.
[35] W. Liu *et al.*, "Power quality assessment in shipboard microgrids under unbalanced and harmonic AC bus voltage," *IEEE Trans. Ind. Appl.*, vol. 55, no. 1, pp. 765–775, Jan./Feb. 2019.
[36] R. Yan and T. K. Saha, "Voltage variation sensitivity analysis for unbalanced distribution networks due to photovoltaic power fluctuations," *IEEE Trans. Power Syst.*, vol. 27, no. 2, pp. 1078–1089, May 2012.
[37] M. Grotzbach and R. Redmann, "Line current harmonics of VSI-fed adjustable-speed drives," *IEEE Trans. Ind. Appl.*, vol. 36, no. 2, pp. 683–690, Mar./Apr. 2000.
[38] A. von Jouanne and B. Banerjee, "Assessment of voltage unbalance," *IEEE Trans. Power Del.*, vol. 16, no. 4, pp. 782–790, Oct. 2001.
[39] C. F. Nascimento *et al.*, "Analysis of noncharacteristic harmonics generated by voltage-source converters operating under unbalanced voltage," *IEEE Trans. Power Del.*, vol. 32, no. 2, pp. 951–961, Apr. 2017.

DAISY H. GREEN (Member, IEEE) received the B.S. degree in electrical engineering from the University of Hawai'i at Mānoa, Honolulu, HI, USA, in 2015, and the M.S. degree and the Ph.D. degree in electrical engineering and computer science from the Massachusetts Institute of Technology (MIT), Cambridge, MA, USA, in 2018 and 2022, respectively.

She is currently a Postdoctoral Associate with the Department of Architecture, MIT. Her research interests include the development of signal processing algorithms for energy management and condition monitoring.

PETER A. LINDAHL (Senior Member, IEEE) received the B.S. degree in electrical engineering from Penn State University, State College, PA, USA, in 2003, and the M.S. degree in electrical engineering and the Ph.D. degree in engineering from Montana State University, Bozeman, MT, USA, in 2009 and 2013, respectively.

He is currently a Manager with the Electrical Engineering Practice, Exponent, Inc., Natick, MA, USA, where he provides technical consulting services in the areas of root-cause failure analysis, product safety and performance assessments, and intellectual property audits for a wide range of electrical, electromechanical, and energy storage systems.

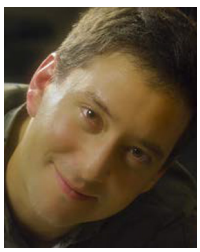

STEVEN B. LEEB (Fellow, IEEE) received the Ph.D. degree from the Massachusetts Institute of Technology (MIT), Cambridge, MA, USA, in 1993.

He has been a member of the MIT Faculty with the Department of Electrical Engineering and Computer Science, MIT since 1993. He also holds a joint appointment with the Department of Mechanical Engineering, MIT. He is concerned with the development of signal processing algorithms for energy and real-time control applications.